A Digital Twin Based Estimation Method for Health Indicators of DC–DC Converters

Yingzhou Peng, *Student Member, IEEE*, Shuai Zhao, *Member, IEEE*, and Huai Wang, *Senior Member, IEEE*

***Abstract*—This article proposes a health indicator estimation method based on the digital-twin concept aiming for condition monitoring of power electronic converters. The method is noninvasive, without additional hardware circuits, and calibration requirements. An application for a buck dc–dc converter is demonstrated with theoretical analyses, practical considerations, and experimental verifications. The digital replica of an experimental prototype is established, which includes the power stage, sampling circuit, and close-loop controller. Particle swarm optimization algorithm is applied to estimate the unknown circuit parameters of interest based on the incoming data from both the digital twin and the physical prototype. Cluster-data of the estimated health indicators under different testing conditions of the buck converter is analyzed and used for observing the degradation trends of key components, such as capacitor and MOSFET. The outcomes of this article serve as a key step for achieving noninvasive, cost-effective, and robust condition monitoring for power electronic converters.**

***Index Terms*—Condition monitoring, dc–dc power converters, digital twin, IGBT, parameter identification, reliability.**

I. Introduction

POWER converters are subject to frequent functional and environmental strains, which can induces failures. The failure mechanisms of power converter are generally separated into two categories: 1) abrupt failure due to over stress conditions; and 2) wearing out and degradation due to long-term operation. The fault diagnosis has been researched for many years to deal with abrupt failures, which is not the content of this article. After long-term operation, some components of power converter become too fragile to withstand the normal electrical and thermal stresses and a collapse of the entire system may happen.

Therefore, the anticipation of the degradation progress of power converter is important and meaningful so the fragile components can be replaced before a breakdown happens and it is called condition monitoring. It is revealed that the degradation progress of the key components in converters can be indicated by the change of their characteristic parameters, such as the ON-state resistance of MOSFET and capacitance of capacitor [1], [2]. Therefore, the measurement of those health indicators is critical and the first step of condition monitoring. Then, data processing method is used to assess the health condition of those key components with considering practical environmental and operational conditions. Overall, condition monitoring could be useful for predictive maintenance based on the estimated degradation level and remaining useful lifetime of the components of interest.

Component-level health indicators have been proposed for monitoring the degradation of power semiconductors and capacitors individually as shown in Table I [3]–[5], which can be classified into two groups: electrical and thermal indicators. Further, electrical indicators can be obtained from either the drain–source/collector–emitter terminals, such as the ON-state voltage or resistance of power semiconductors, which can be measured by using measurement circuits [1], [6]–[8]. These indicators show higher sensitivity to the degradation of power semiconductors among existing indicators. But additional circuits are needed, which increases the implementation complexity. Existing gate-emitter related indicators includes the threshold voltage and miller plateau of power semiconductor, which can be obtained from the gate turn-ON transient voltage waveform [9]–[12]. Since junction temperature is strongly related to the health condition of power semiconductors, temperature sensitive electrical parameters (TSEPs) can also be used as health indicator, such as prethreshold voltage in [13], peak gate current in [14], Kelvin-emitter voltage [15], and switching time in [16]. However, all of these gate related indicators are high frequency signals, demanding the high speed data acquisition circuit with good noise-immune ability, which increases the complexity further. Moreover, the malfunction of the added circuit may induce the failure of the gate driver. Thermal signals are also proposed for condition monitoring, such as case temperature in [17] and [18] and thermal resistance in [19]. However, case temperature may be easily interfered by other heat sources (e.g., the neighboring power modules and components, the ambient temperature) and shows a low degradation sensitivity. The measurement of thermal resistance strongly depends on the accuracy of measuring junction temperature, case temperature and power losses of interested module, which is complicated and difficult.

As for the capacitor, the condition monitoring can be achieved through two ways: 1) taking advantage of the discharge process of capacitor when the power converter is in offline [20]; and 2) by measuring the ripple of capacitor voltage and current, the

Manuscript received November 27, 2019; revised February 16, 2020, April 27, 2020, and June 10, 2020; accepted July 3, 2020. Date of publication July 15, 2020; date of current version September 22, 2020. This work was supported by the Innovation Fund Denmark through the Advanced Power Electronic Technology and Tools (APETT) Project 6154-00010B. Recommended for publication by Associate Editor P. Mattavelli. *(Corresponding author: Yingzhou Peng.)*

The authors are with the Department of Energy Technology, Aalborg University, 9220 Aalborg, Denmark (e-mail: ype@et.aau.dk; szh@et.aau.dk; hwa@et.aau.dk).

Color versions of one or more of the figures in this article are available online at https://ieeexplore.ieee.org.

Digital Object Identifier 10.1109/TPEL.2020.3009600

TABLE I
CONVENTIONAL CONDITION MONITORING METHODS

Items	Measured signals	Health indicators	Implementation complexity	Sensitivity to degradation	Invasion to original system
Component-level (power semiconductor)	Electrical signals	On-state voltage [6]–[8]	+++	++++	+++
		On-state resistance [1]	+++	++++	+++
		Threshold voltage [9]	++++	+++	++++
		Miller plateau [10], [11]	++++	+++	++++
		TSEPs [13]–[16]	++++	+++	++++
	Thermal signals	Case temperature [17], [18]	+	+	++
		Thermal resistance [19]	++++	++++	+++
Component-level (capacitor)	Discharge process	Capacitor voltage [20]	++	+++	+
	Capacitor voltage and current ripple	Capacitance and ESR [2], [21]–[23]	++++	++	+++
System-level (single component)	System signals	Frequency response [24]	++++	+	+++
		Harmonic [25]	++++	+	++++
		ANN [26], [27]	++++	++	+
System-level (multi-components)	System signals	Parameter identification [28]–[31]	++	++	+++
Data process	Calibration [6]	Indicators are also sensitive to temperature and current, they need to be calibrated.			
	Noise reduction [32], [33]	The measured indicators may consist of massive noises.			

TSEPs: temperature sensitive electrical parameters. ANN: artificial neural network. ESR: equivalent series resistance

equivalent series resistance (ESR) and capacitance of the capacitor can be obtained [2], [21]. However, in practice, obtaining the ripple requires more steps. First, capacitor current is measured indirectly by combining the input current, output current, and the switching information of the power converter [22], [23], which may cause transfer errors. Then, measuring the ripple requires both the data acquisition apparatus with higher sampling rate and higher resolution, and high frequency pass filter circuit.

From the system-level view, various methods have been proposed to monitor the power semiconductors and capacitors, respectively, as listed in Table I. The frequency response of dc–dc converters is sensitive to the ON-state resistance of power semiconductors in specific situations [24]. In addition, the output current harmonic of inverter is investigated to monitor the degradation of the solder layer of power semiconductor in [25]. Both methods require extra setups and show invasive to the system of interest. Moreover, they cannot distinguish the degradation of power semiconductor and capacitor. Artificial neural network is also a potential way for monitoring the degradation of capacitor [26], [27]. However, it requires offline testing to obtain the enough training data, which is difficult to achieve in practice.

Conventional model-based parameter identification methods are used to modify the controller of power converters as listed in Table I. It is known that the transfer function between the output voltage and duty cycle ratio is discretized when design controller. Thus, the coefficients of transfer function can be calculated by using different algorithms, such as recursive least square (RLS) in [28] and Kalman filter (KF) in [29], which is effective in tuning controller and improving the system performance. However, mapping the coefficients of transfer function into the internal parameters of the converter could cause transfer errors and even does not have feasible solutions when the number of unknown parameters are more than that of the known equations. In [31], a simplified model of boost converter is built and a generalized gradient descent algorithm is applied to calculate the inductance and capacitance. A model for buck converter is developed in [30], where biogeography-based optimization method is used to identify the internal parameters. The main issues with the above methods are that none of them focus on the degradation monitoring of the key components. Moreover, only the coefficients of the model (e.g., transfer function) or part of those physical parameters (e.g., inductance and capacitance) can be obtained. In addition, all of the above methods need to inject extra signal into the controller.

It is worth to mentioning that these measured indicators need to be processed further to reduce noises and to indicate the health status of power converter numerically. Such as low-pass filter and Gaussian process [32], [33]. Finally, calibration with other impactors (e.g., temperature and current) is needed as well. [6].

According to the analysis above, the challenges are still existed in these existing methods and they are expected to updated with the features of noninvasive, calibration-free, without additional circuits and the ability of monitoring both power semiconductor and capacitor.

Digital twin is a virtual representation of a physical system that virtually shares the same characteristics with its physical counterpart. It enables customers to better understand, optimize, predict, and monitor the performance of its installed systems [34], [35]. The concept of digital twin has been applied in power converters for fault diagnosis recently [36], [37], which is achieved by comparing the output signals of the digital twin and its physical counterpart in real-time. In this article, the digital twin concept is used to estimate the health indicators of the key components in power converter, so as the degradation progress of power converter can be monitored. The digital twin technology includes two parts: the digital presentation of a physical system and an advanced algorithm for data analysis.

First, a digital twin concept-based health indicator estimation method is proposed for a dc–dc converter case study. This digital twin is a virtual replica of physical converter and is able to update itself continuously according to the data coming from existing sensors in its physical counterpart. Then, PSO algorithm is applied to do data analysis and make the difference between the digital twin and its physical counterpart smaller than a preset threshold. Finally, a data-cluster concept is proposed to cover the estimated indicators at different possible operations.

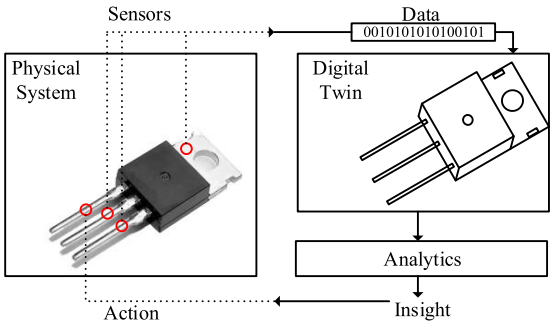

Fig. 1. Example of the application of digital twin.

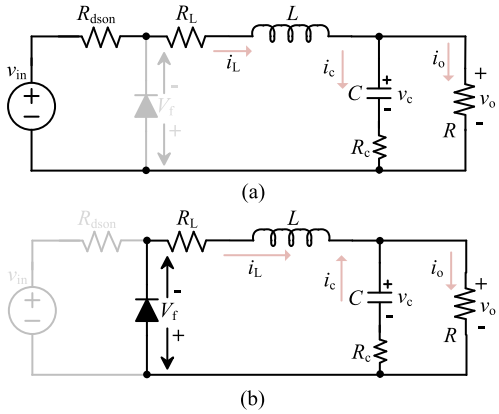

Fig. 2. Equivalent circuits of buck converter: (a) MOSFET is in ON-state; (b) MOSFET is in OFF-state.

The contributions of this article are: 1) it is easy to implement by taking advantage of existing sensors; 2) without additional hardware and modification in the system of interest; 3) it is capable of monitoring the degradation of the key components simultaneously; and 4) by taking advantage of cluster-data based method to achieve the calibration-free and compensate the shortage of the proposed method in the low sensitivity to degradation. Part of the contents of this article have been presented in [38], which mainly discussed the basic idea of the proposed method. In this article, the state-of-the-arts discussion is enriched by considering component-level, system-level, single component, and multicomponents based condition monitoring methods. Moreover, the detail of the digital twin concept is illustrated through a MOSFET-based example and the experimental validation is carried out in a buck converter demonstrator with practical considerations, such as different voltages, currents, loadings, and temperatures. In addition, a data analysis method is also given in this article.

II. Digital Twin of Buck Converter

A. Digital Twin Concept

An example of MOSFET-based digital twin is taken to illustrate the principle of digital twin first as shown in Fig. 1 with seven components and they are explained as follows.

1) *Physical system:* A real physical object or process.
2) *Sensors:* Sensors are used to capture the operational signals of physical system, which could be voltage, current or temperature, etc.
3) *Data:* The data from the sensors represent the operational condition or characteristics of physical system and they are used to update the digital twin continuously.
4) *Digital twin:* A digital replica of physical system.
5) *Analytics:* Analytics techniques are used to process the data from the sensors by using advanced algorithms and make the insights of digital twin same with the insights of its physical counterpart as much as possible.
6) *Insight:* The inside information of digital twin. The insights could be used to guide the action of physical system and better its performance. Also, it can be used to assess the operation condition of physical system.
7) *Action:* According to the insights from analytics, action could be performed to better the performance of physical system or protect the physical system.

B. Buck Converter Modeling

Fig. 2 shows the equivalent circuits of buck converter operating at ON-state and OFF-state, which is represented by

$$\begin{bmatrix} \frac{di_L}{dt} \\ \frac{dv_c}{dt} \\ v_o \end{bmatrix} = \begin{bmatrix} -\frac{1}{L}A & -\frac{1}{L}\left(\frac{R}{R_c+R}\right) \\ \frac{1}{C}\left(\frac{R}{R_c+R}\right) & -\frac{1}{C}\left(\frac{1}{R_c+R}\right) \\ \frac{R_cR}{R_c+R} & \frac{R}{R_c+R} \end{bmatrix} \times \begin{bmatrix} i_L \\ v_c \end{bmatrix} + D\begin{bmatrix} \frac{1}{L}v_{in} \\ 0 \\ 0 \end{bmatrix} + (1-D)\begin{bmatrix} -\frac{1}{L}V_f \\ 0 \\ 0 \end{bmatrix}$$

$$A = \left(DR_{dson} + R_L + \frac{R_cR}{R_c+R}\right) \tag{1}$$

where i_L is the inductor current, v_o is the output voltage and v_c is the capacitor voltage; R_{dson}, R_L, and R_C are the parasitic resistances of MOSFET, inductor and capacitor, respectively; v_{in} is the input voltage and V_f is the forward voltage of diode; and D is 1 when the MOSFET is ON and 0 when the MOSFET is OFF.

Two ways can be applied to solve (1), and obtain i_L and v_c. One is to calculate the eigenvector and eigenvalue of differential equations and construct the general solution. Then, by using the initial values of i_L and v_c, the specific solution of these differential equations can be obtained [30]. This method demands heavy computation, especially the calculation of eigenvector and eigenvalue. The other one is to linearize the differential equations with acceptable accuracy, which is used in this article. Then, the output voltage v_o can be described with discrete time step

$$v_{o,n+1} = i_{L,n+1}\frac{R_cR}{R_c+R} + v_{c,n+1}\frac{R}{R_c+R} \tag{2}$$

where the nth time step is defined as the present time interval, and the $(n+1)$th time step represents the next one. $v_{o,n+1}$ indicates the output voltage at $(n+1)$th step, which is unknown at present nth step. Therefore, in the following discussions, $i_{L,n+1}$ and $v_{c,n+1}$ are derived based on the present values $i_{L,n}$ and $v_{c,n}$,

so that the output voltage at the $(n+1)$th time step can be represented by the inductor current and capacitor voltage at nth time step.

Runge–Kutta is a typical method to solve differential equations [39]. A typical fourth-order Runge–Kutta method is used in this article to linearize the differential equations and it is considered as sufficient for buck converter modeling to achieve an negligible error. To simplify the analysis process, (1) is rewritten as follows:

$$\begin{cases} f_1(i_{\mathrm{L}}, v_{\mathrm{c}}) = \dfrac{di_{\mathrm{L}}}{dt} \\ f_2(i_{\mathrm{L}}, v_{\mathrm{c}}) = \dfrac{dv_{\mathrm{c}}}{dt}. \end{cases} \tag{3}$$

With fourth-order Runge–Kutta method, $i_{\mathrm{L,n+1}}$ and $v_{\mathrm{c,n+1}}$ can be expressed as follows:

$$\begin{cases} i_{\mathrm{L,n+1}} = i_{\mathrm{L,n}} + \dfrac{h}{6}\left(k_{\mathrm{a1}} + 2k_{\mathrm{a2}} + 2k_{\mathrm{a3}} + k_{\mathrm{a4}}\right) \\ v_{\mathrm{c,n+1}} = v_{\mathrm{c,n}} + \dfrac{h}{6}\left(k_{\mathrm{b1}} + 2k_{\mathrm{b2}} + 2k_{\mathrm{b3}} + k_{\mathrm{b4}}\right) \end{cases} \tag{4}$$

where k_{a1}-k_{a4} and k_{b1}-k_{b4} are used to calculate the average change rate between (n)th and $(n+1)$th step shown as follows:

$$\begin{cases} k_{\mathrm{a1}} = f_1\left(x_{\mathrm{n}}, y_{\mathrm{n}}\right) \\ k_{\mathrm{b1}} = f_2\left(x_{\mathrm{n}}, y_{\mathrm{n}}\right) \\ k_{\mathrm{a2}} = f_1\left(x_{\mathrm{n}} + \dfrac{h}{2}k_{\mathrm{a1}}, y_{\mathrm{n}} + \dfrac{h}{2}k_{\mathrm{b1}}\right) \\ k_{\mathrm{b2}} = f_2\left(x_{\mathrm{n}} + \dfrac{h}{2}k_{\mathrm{a1}}, y_{\mathrm{n}} + \dfrac{h}{2}k_{\mathrm{b1}}\right) \\ k_{\mathrm{a3}} = f_1\left(x_{\mathrm{n}} + \dfrac{h}{2}k_{\mathrm{a2}}, y_{\mathrm{n}} + \dfrac{h}{2}k_{\mathrm{b2}}\right) \\ k_{\mathrm{b3}} = f_2\left(x_{\mathrm{n}} + \dfrac{h}{2}k_{\mathrm{a2}}, y_{\mathrm{n}} + \dfrac{h}{2}k_{b2}\right) \\ k_{\mathrm{a4}} = f_1\left(x_n + hk_{\mathrm{a3}}, y_{\mathrm{n}} + hk_{\mathrm{b3}}\right) \\ k_{\mathrm{b4}} = f_2\left(x_n + hk_{\mathrm{a3}}, y_{\mathrm{n}} + hk_{\mathrm{b3}}\right) \end{cases} \tag{5}$$

where h is the calculation step time between nth and $(n+1)$th time step.

Substitute (3) into (5), (5) into (4), and (4) into (2), the final expression of v_{o} can be obtained as:

$$\begin{cases} v_{\mathrm{o,n+1}} = ai_{\mathrm{L,n}} + bv_{\mathrm{c,n}} + c \\ a = f_3(L, C, R_{\mathrm{L}}, R_{\mathrm{C}}, R_{\mathrm{dson}}) \\ b = f_4(L, C, R_{\mathrm{L}}, R_{\mathrm{C}}, R_{\mathrm{dson}}) \\ c = f_5(L, C, R_{\mathrm{L}}, R_{\mathrm{C}}, R_{\mathrm{dson}}) \end{cases} \tag{6}$$

where coefficients a, b, and c are constructed by seven parameters (L, C, R_{L}, R_{C}, R_{dson}, D, and v_{in}) with complicated combinations since there are five layers substitution from (3) to (2). Among them, L, C, R_{L}, R_{C}, and R_{dson} are unknown parameters. D is calculated through the sampling circuit model and close-loop controller model described later. v_{in} is measured from the physical converter. Therefore, the output voltage at $(n+1)$th step can be calculated by using the inductor current and capacitor voltage at nth step. Then, v_{o} is used to determine the ON–OFF state of MOSFET D through the following sampling circuit and close-loop controller model.

C. Sampling Circuit

A typical sampling circuit is adopted, which includes a differential amplifier circuit and a $R_{\mathrm{f}}C_{\mathrm{f}}$ low-pass filter as shown in Fig. 3. The amplifier output voltage v_{p} is

$$v_{\mathrm{p,n+1}} = \frac{(R_3 + R_4)R_2}{(R_1 + R_4)R_5} v_{\mathrm{o,n+1}}. \tag{7}$$

The output of $R_{\mathrm{f}}C_{\mathrm{f}}$ filter v_{ad} is

$$\begin{cases} v_{\mathrm{ad,n+1}} = v_{\mathrm{p}} - R_{\mathrm{f}}C_{\mathrm{f}}\dfrac{dv_{\mathrm{ad,n+1}}}{dt} \\ f_6(v_{\mathrm{ad,n+1}}) = \dfrac{dv_{\mathrm{ad,n+1}}}{dt} = \dfrac{v_{\mathrm{p}} - v_{\mathrm{ad,n+1}}}{R_{\mathrm{f}}C_{\mathrm{f}}}. \end{cases} \tag{8}$$

Based on fourth-order Rung–Kutta method, (8) can be linearized as follows:

$$\begin{cases} v_{\mathrm{ad,n+1}} = v_{\mathrm{ad,n}} + \dfrac{h}{6}\left(k_1 + 2k_2 + 2k_3 + k_4\right) \\ k_1 = f_3\left(y_{\mathrm{n}}\right) \\ k_2 = f_3\left(y_{\mathrm{n}} + \dfrac{h}{2}k_1\right) \\ k_3 = f_3\left(y_{\mathrm{n}} + \dfrac{h}{2}k_2\right) \\ k_4 = f_3\left(y_{\mathrm{n}} + hk_3\right). \end{cases} \tag{9}$$

D. Close-Loop Controller

To obtain modulation signal v_{m}, the close-loop controller is built in digital twin as shown in Fig. 3. The process of controller can be expressed by following linear equations:

$$\begin{cases} v_{\mathrm{e,n}} = v_{\mathrm{e,n+1}} \\ v_{\mathrm{m,n}} = v_{\mathrm{m,n+1}} \\ v_{\mathrm{e,n+1}} = V_{\mathrm{ref}} - v_{\mathrm{ad,n+1}} \\ v_{\mathrm{m,n+1}} = v_{\mathrm{m,n}} + K_{\mathrm{p}}(v_{\mathrm{e,n+1}} - v_{\mathrm{e,n}}) + K_I h v_{\mathrm{e,n+1}} \end{cases} \tag{10}$$

where V_{ref} is the reference of the output voltage, v_{e} is the error between the output voltage and its reference, v_{m} is the modulation signal, and K_{P} and K_{I} are the parameters of the PI controller. Based on (10), the digital twin of buck converter can generate the modulation signal by itself instead of accessing to the physical controller. It is worth to mentioning that the sampling rate of physical buck converter system is usually set to the switching frequency and the time delay in updating the duty cycle ratio should be considered.

Then, the ON–OFF state of MOSFET D is decided by comparing v_{m} with a triangular carrier signal v_{tri} as follows:

$$D_{\mathrm{n+1}} = \begin{cases} 1(v_{\mathrm{m,n+1}} \geq v_{\mathrm{tri,n+1}}) \\ 0(v_{\mathrm{m,n+1}} < v_{\mathrm{tri,n+1}}). \end{cases} \tag{11}$$

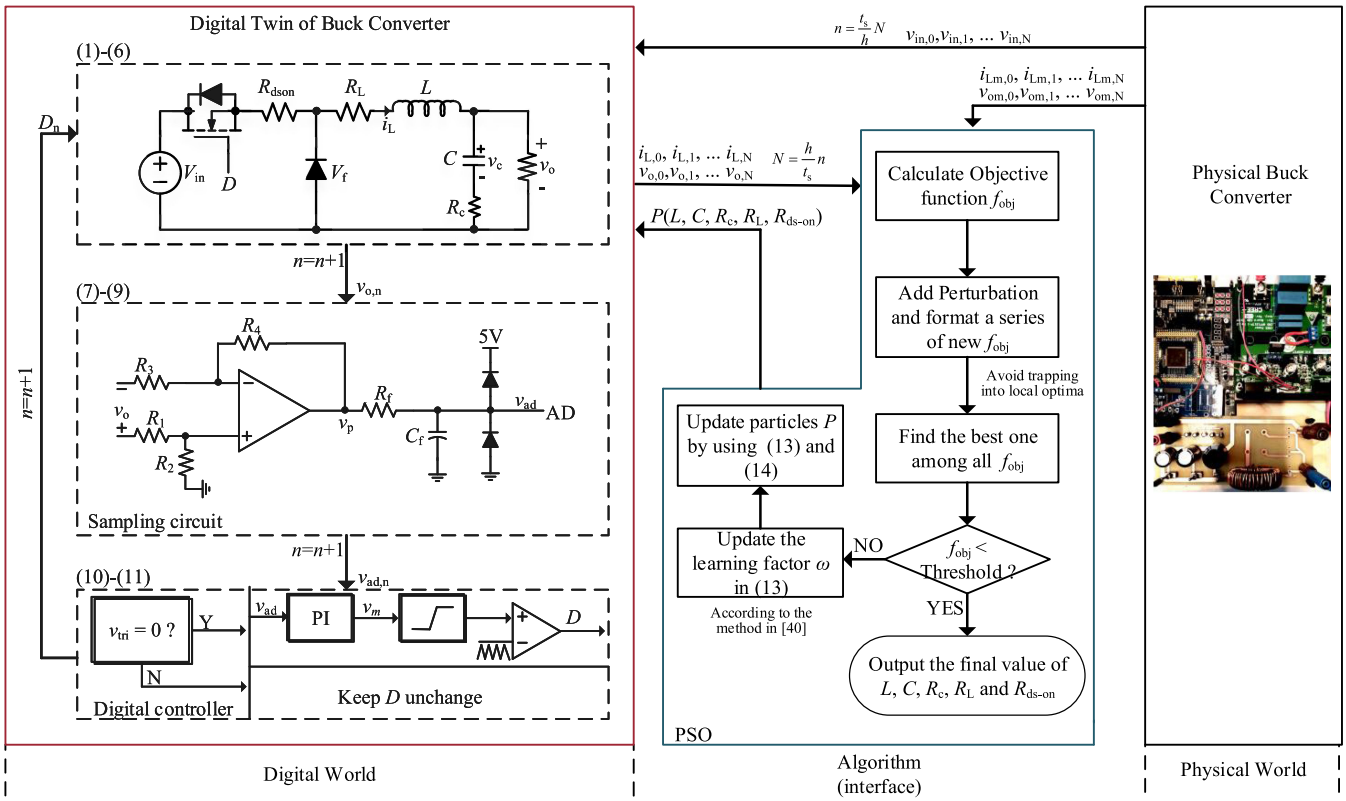

Fig. 3. Case study of the application of digital twin concept in condition monitoring with a buck converter ($n = n + 1$ means updating the time step, R_1–R_4, R_f, and C_f are the parameters of sampling circuit, v_{tri} is the triangular carrier, f_{obj} is the objective function, w is the learning factor in (13), N is the number of sampled output voltage and inductor current from physical converter, n is the total iteration steps of the digital twin for updating parameters one time, t_s is the sampling period of measuring output voltage, inductor current, and input voltage from physical converter, and h is the calculation time step interval inside the digital twin).

III. Application of Digital Twin in Condition Monitoring

The final model of the buck converter developed in this article is expressed by (6). It can be seen that the coefficients a, b, and c are highly nonlinear functions with five variables. Therefore, the traditional algorithms, like RLS and KF, are not able to estimate the developed model in this article [40]. Further, the extended Kalman filter (EKF) is proposed to solve the nonlinear problem. However, It suffers instability due to the linearization and costly derivative calculation of Jacobian or Hessian matrices, and its performance deteriorates when the signal model is highly nonlinear [41]. More importantly, a critical point during the design of EKF and unscented Kalman filter is the determination of the covariance matrices of the process noise, the measurement noise, and the initial state vector, which are often estimated from a tedious trail-and-error tuning or self-tuning algorithms [29], [40], [42]. Considering the complex process and restrictions of EKF, PSO is chosen in this article because it is an end-to-end solution, and has a simpler implementation process and better generality to different models. It is agreed that PSO requires more computation than KF-based algorithms. But the computation time of the algorithm is not critical in the application presented here, since the degradation of power electronic components is a slow process itself.

PSO is a population-based iterative optimization algorithm that mimics the swarm behavior in birds flocking and fish schooling to guide the particles to search for the globally optimal solutions [43]. Based on this, it is possible to search for the optimal solutions of the internal parameters of digital twin buck converter. To implement PSO, the first step is to construct an objective function. In this article, the objective function is as follows:

$$f_{\text{obj}} = \frac{\sum_{j=1}^{N}\left[\left(i_{\text{L,j}} - i_{\text{Lm,j}}\right)^2 + \left(v_{\text{o,j}} - v_{\text{om,j}}\right)^2\right]}{N} \tag{12}$$

where $i_{\text{L,j}}$ and $v_{\text{o,j}}$ are, respectively, the calculated inductor current and output voltage from the digital twin buck converter. $i_{\text{Lm,j}}$ and $v_{\text{om,j}}$ are the measured data from the physical buck converter, and N is the sample size of the measured data. The internal parameters of physical buck converter can be obtained by minimizing the objective function defined in (12) with PSO algorithm.

The procedure of the proposed digital twin-based condition monitoring method is shown in Fig. 3, which includes three parts: digital world, physical world, and the interface (PSO algorithm) between them. P represents the parameter set including L, C, R_c, R_L, and R_{dson}. First, the parameter set P, i_L, v_c, and the ON–OFF state D are initialized and n is 0 at the beginning

time step. Then, the inductor current i_{L}, capacitor voltage v_{c}, and output voltage v_{o} at next step can be calculated through (4) and (6), and the time step is updated by $n = n + 1$. Finally, D is updated through the developed sampling circuit and close-loop controller model and sent back into converter model to do next loop calculation.

Because the calculation time step h is different with the sampling period t_{s}. The number of calculated i_{L} and v_{o} n is reduced to N by $N = hn/t_{\mathrm{s}}$ evenly. Then, the calculated i_{L} and v_{o} sets from the digital twin and the measured i_{Lm} and v_{om} sets from the physical one are used to calculate f_{obj} by (12). Thereafter, perturbation mechanism is added to avoid trapping into local optima by constructing a series of new f_{obj}. After that, the best f_{obj} among all f_{obj} is found. If the f_{obj} is smaller than the preset threshold, the output parameter set from the digital twin represents the operational condition of physical buck converter. Otherwise, the parameter set will be updated by the following equations:

$$V_{\mathrm{i,j}} = \omega_{i-1} V_{\mathrm{i-1,j}} + 2r_{1,\mathrm{i-1,j}} \left(P_{\mathrm{G}} - P_{\mathrm{i-1,j}}\right) + 2r_{2,\mathrm{i-1,j}} \left(P_{\mathrm{L,i-1,j}} - P_{\mathrm{i-1,j}}\right) \quad (13)$$

$$P_{\mathrm{i,j}} = P_{\mathrm{i-1,j}} + V_{\mathrm{i,j}} \quad (14)$$

where i is the number of iteration, j is the number of particle, $V_{\mathrm{i,j}}$ is the moving velocity of the jth particle in ith iteration; P_{G} is the global optimization, $P_{\mathrm{L,i-1,j}}$ is the individual optimization of the jth particle until $(i-1)$th iteration; $P_{i,j}$ is the position of the jth particle in ith iteration; and w is the learning factor that is updated continuously according to the method presented in [43]. r_1 and r_2 are weighting factors and are set to 2. The detail about how to chose these factors can be found in [43].

Finally, the new obtained P is sent back into the digital twin of buck converter to do next step calculation.

In addition, the converging process of PSO may trap into local optima. To avoid this, a proper perturbation is needed. In this article, after obtaining the global optimization P_{G} in each iteration, a perturbation factor is introduced to construct a series of new particles. Then, a series of new f_{obj} can be obtained. The detail of the perturbation process can be see in [44].

IV. Application for Condition Monitoring and Experimental Validation

To validate the proposed method, a buck converter demonstrator is built, as shown in Fig. 4(a), and its specifications are presented in Table II. The LC filter module is built by using several different inductors and capacitors, then they can be switched easily during test. This article leverages the load change transients, which is relevant to many practical applications. The example waveforms are shown in Fig. 4(b) and part of the waveform data are used in this article.

A. Parameter Identification

By following the procedure shown in Fig. 3, the parameters of buck converter can be obtained. Fig. 5(a) shows the descending process of f_{obj} and its final value is 6e-4 after 50 generations. Meanwhile, these parameters converge to a stable value after 50 generations as illustrated in Fig. 5(b) and (c), which means the

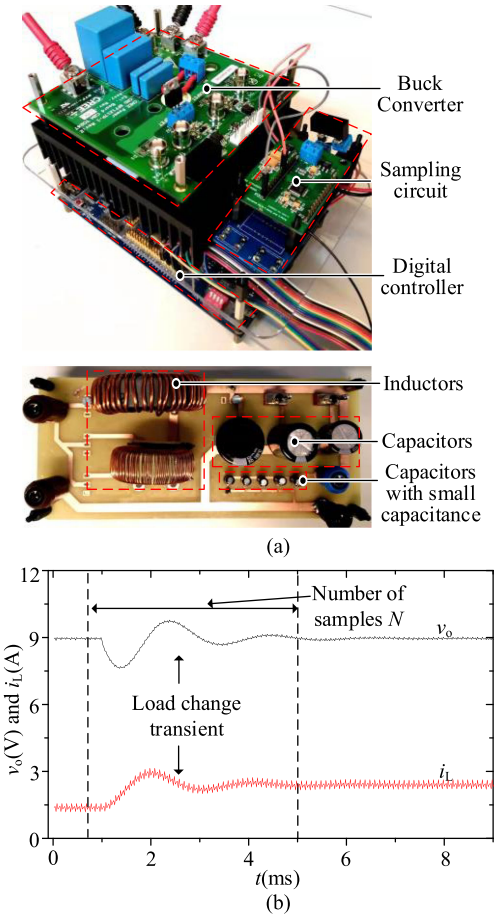

Fig. 4. Experimental setup. (a) Physical buck converter system. (b) Load change transient waveforms of i_{L} and v_{o}.

TABLE II
Specifications of Buck Converter

Specification	Value
$V_{\mathrm{in}}/V_{\mathrm{ref}}$	24 V/9 V
$V_{\mathrm{in}}/V_{\mathrm{ref}}$	48 V/24 V
$V_{\mathrm{in}}/V_{\mathrm{ref}}$	110 V/24 V
Switching frequency f_{sw}	20 kHz
Loading 1/2/3	10.4 Ω / 4.9 Ω/ 3.3 Ω
L (μH)	782
C (μF)	151

difference of the output waveforms between the digital twin buck converter and its physical counterpart is 6e-4. At this moment, these estimated parameters represent the condition of physical buck converter.

The comparisons of i_{L} and v_{o} between the digital twin buck converter and the physical one are shown in Fig. 6. It can be seen that the waveforms are almost overlapped with each other in both dynamic and static responses, which indirectly prove that the estimated parameters by using the proposed method are very close to the real parameters in the physical one.

For condition monitoring, practical issues should be considered. In the rest of this article, the impact of sampling rate, the uncertainty caused by errors, the different voltage conversions, loadings, and temperatures are discussed. Simultaneously

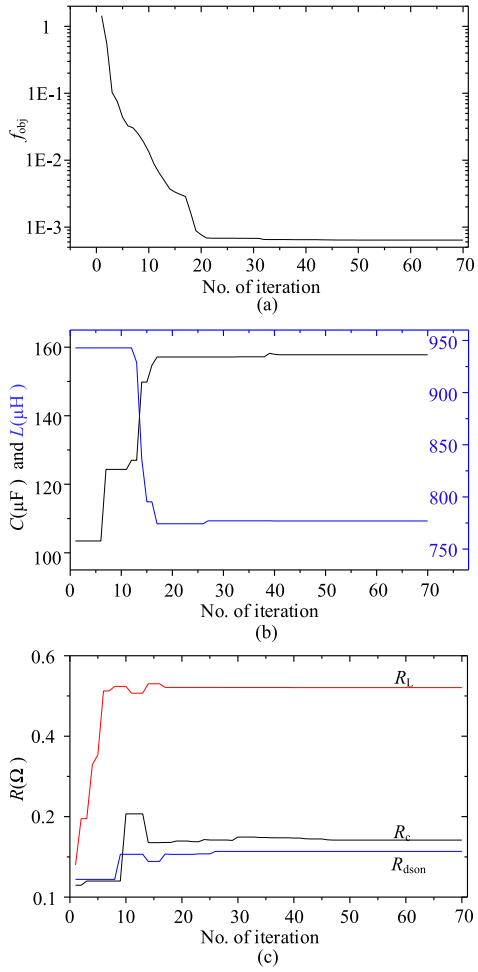

Fig. 5. Process of parameter convergence. (a) Descent process of objective function. (b) Capacitance and inductance. (c) Parasitic resistances R_{L}, R_{c} and R_{dson}.

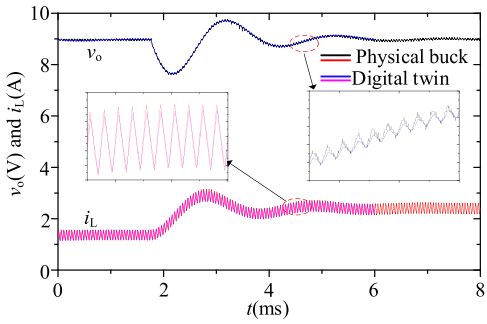

Fig. 6. Comparisons of inductor current and output voltage between digital twin buck converter and its physical counterpart (sampling rate = 1 MHz).

parameter degradation monitoring for capacitor and MOSFET is investigated quantitatively as well.

B. Impact of Sampling Rate

The digital twin works as a sensor-enabled digital model of a physical system. Thus, the sampling rate may affect the accuracy

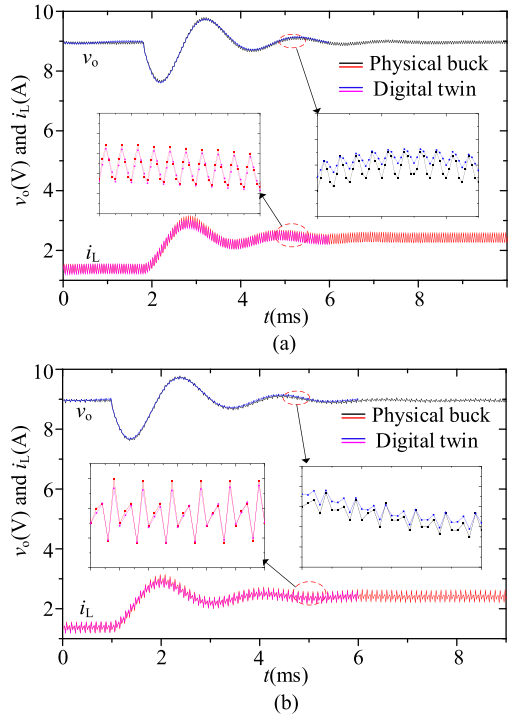

Fig. 7. Comparisons of inductor current and output voltage between digital twin buck converter and its physical counterpart in different sampling rate (the situation when f_{sr} = 1 MHz is presented in Fig. 6): (a) f_{sr} = 100 kHz; (b) f_{sr} = 50 kHz.

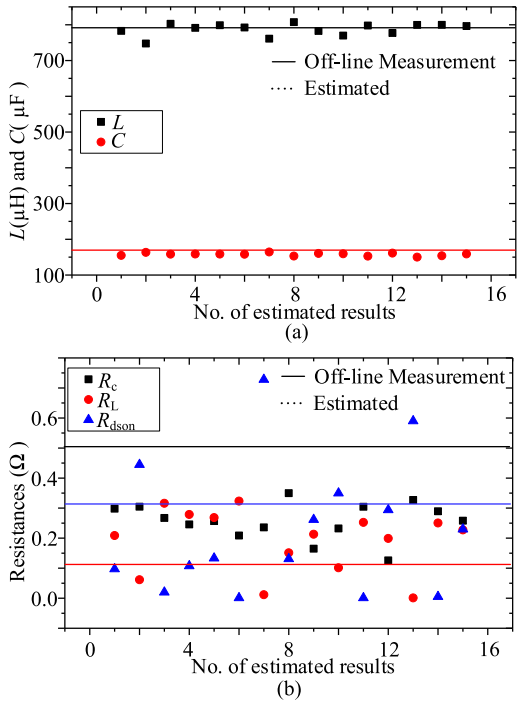

Fig. 8. Estimated results when $V_{\mathrm{in}}/V_{\mathrm{o}}$ is 24/9 V and the load is changed from 4.85 to 3.32 Ω, and the measured results offline (the proposed method is repeated for 15 times to show the fluctuation of estimated results, but the load change transient data is measured for only 1 time. The R_{dson} is measured offline by conducting a certain current). (a) Inductance and capacitance. (b) Parasitic resistances.

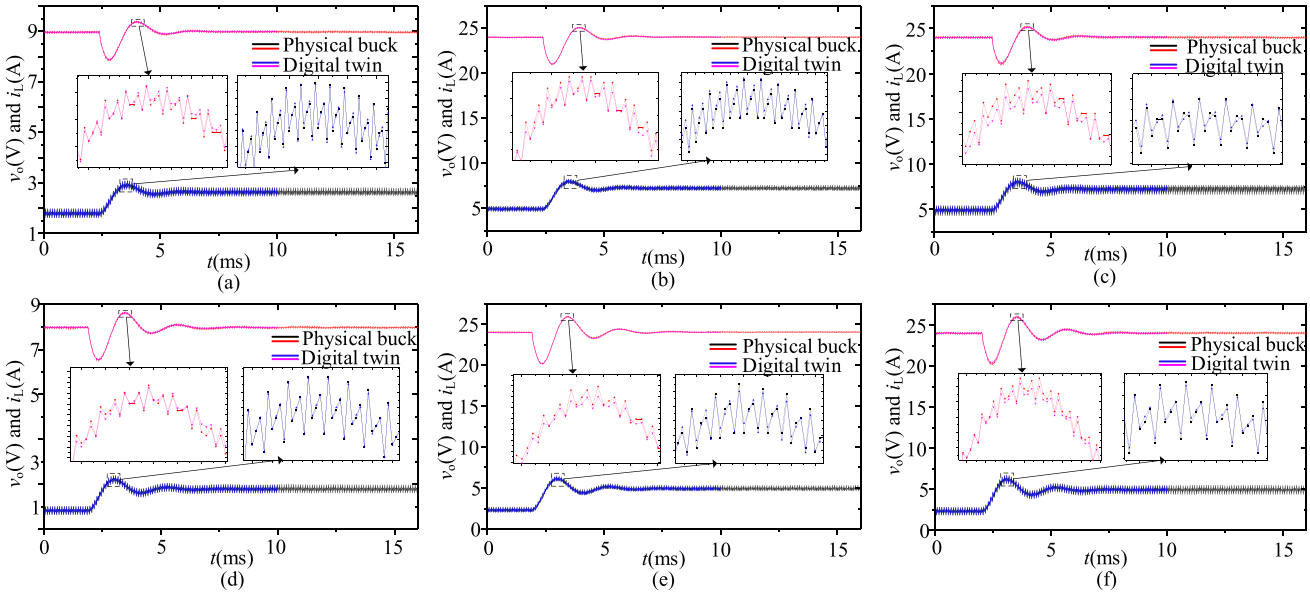

Fig. 9. Comparisons of the output waveforms between the digital twin and its physical counterpart in different operational conditions: (a) case1; (b) case3; (c) case5; (d) case2; (e) case4; (f) case6.

of the results of the digital twin. To uncover this, the proposed method is performed in different sampling rate situations and the results are shown in Fig. 7 (the situation when $f_{\rm sr} = 1$ MHz is presented in Fig. 6). With different sampling rate, the ripples of $i_{\rm L}$ and $v_{\rm o}$ in digital twin and physical one are different. However, they show the same result in dynamic responses. it is known that inductance and capacitance are sensitive to the dynamic responses of $i_{\rm L}$ and $v_{\rm o}$, while the parasitic resistances are sensitive to the ripples of $i_{\rm L}$ and $v_{\rm o}$. Therefore, lower sampling rate could cause higher measurement errors in the ripples of $i_{\rm L}$ and $v_{\rm o}$, which may lead to errors in estimating the results of parasitic resistances.Therefore, to sense the change of the switching ripple, a sampling rate with at least double switching frequency is needed, as shown in Fig. 7(b). In the rest of this article, 50 kHz sampling rate is chosen to acquire $i_{\rm L}$ and $v_{\rm o}$.

TABLE III
DIFFERENT OPERATIONAL CONDITIONS

Cases	$V_{\rm in}/V_{\rm o}$ (V)	Load change (Ω)
case1	24/9	4.85/3.32
case2	24/9	10.43/4.85
case3	48/24	4.85/3.32
case4	48/24	10.43/4.85
case5	110/24	4.85/3.32
case6	110/24	10.43/4.85

C. Impact of Errors

To investigate the consistency of the proposed method, Fig. 8 includes the results of the estimated inductance, capacitance, and parasitic resistances for 15 repeated estimations. It can be noted that the estimated capacitance and inductance exhibit smaller fluctuation along with the results measured offline (LC and their parasitic resistances are measured by *LCR* meter, $R_{\rm dson}$ is measured by conducting a certain current), compared to that of parasitic resistances, since the capacitor and inductor are more sensitive to the load dynamics of the buck converter. Among parasitic resistances, the estimated result of $R_{\rm c}$ is more stable than the results of $R_{\rm L}$ and $R_{\rm dson}$. Because the inductor and MOSFET in buck converter can be seen as in series, which is discussed in the part F of Section IV. Overall, the certain level of estimation errors exist with the proposed method and are caused by: 1) the developed digital twin without considering the parasitic parameters of wires; 2) the sampling circuit without sensing very accurate voltage and current; 3) the different processor of close-loop controller between physical buck converter (DSP) and digital twin (computer); and 4) in relative to the results measured offline, those parameters experience changes when the converter is in operation.

D. Impact of Environmental and Operation Conditions

In practice, the environmental and operation conditions can also affect the values of the health indicators, besides the degradation level of the components of interest, which is a common issue to various condition monitoring methods to date. Moreover, as shown in Fig. 8, there are certain level of estimation errors. One way to address the issue is to calibrate the components of interest at different environmental and operation conditions, as applied in [6] and [7]. Nevertheless, it is time consuming and may not be practical by considering that it is necessary to calibrate each components in each produced unit due to the initial parameter variations among a population of units. In order to avoid the calibration process, this article proposes a data-cluster based method for condition monitoring.

To achieve this, the proposed method is tested in six different operational conditions as listed in Table III. The corresponding results are depicted in Fig. 9, showing that the proposed digital

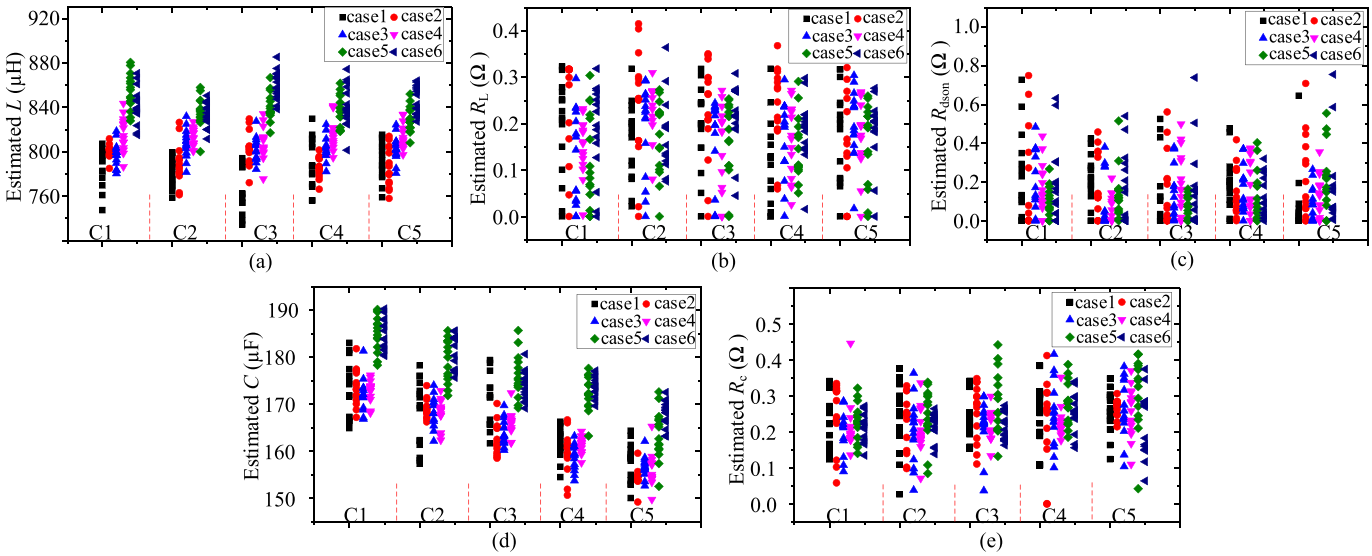

Fig. 10. Estimated results in different operational cases and when C is manually decreased from C1 to C5 (here MOSFET M1 is applied. case 1–6 are described in Table III, C1–C5 are described in Table IV): (a) L; (b) $R_{\rm L}$; (c) $R_{\rm dson}$; (d) C; (e) $R_{\rm c}$.

TABLE IV
PERCENTAGE CHANGE OF CAPACITANCE DURING TEST

Caps	C1	C2	C3	C4	C5
$\Delta\ C$	0% (165 μF)	-2.2%	-4.4%	-6.6%	-8.8%

TABLE V
ON-STATE RESISTANCES OF THE MOSFETS UNDER TEST

MOSFETs	M1	M2	M3	M4	M5
$R_{\rm dson}$ (Ω)	0.11	0.241	0.385	0.495	0.75

TABLE VI
CASE TEMPERATURE OF THE MOSFETS UNDER TEST IN DIFFERENT OPERATIONAL CONDITIONS (UNIT: °C)

Cases	$T_{\rm c-M1}$	$T_{\rm c-M2}$	$T_{\rm c-M3}$	$T_{\rm c-M4}$	$T_{\rm c-M5}$
case1	27.5	27.8	28	28.8	28.3
case2	25.7	26.8	26.5	27.1	26.5
case3	29	39.4	40.9	44	55
case4	26.5	29.1	29.3	32.8	34.8
case5	28.4	32.4	36.7	37.3	39.5
case6	26.1	27.5	28.4	29.7	30.8

twin is able to present the similar operation characteristics with its physical counterpart even in different operational conditions. The identified parameters are given in next section. In this article, five capacitances and five MOSFETs are used to simulate the degradation level of capacitor and MOSFET as listed in Tables IV and V, respectively. It should be noted that the case temperatures of MOSFETS are different in operation due to the different power losses as recorded in Table VI.

E. Capacitor Degradation Monitoring

It has been revealed that the capacitance may drop by 5%–20% after a long-term operation [5]. Therefore, in this article, another four capacitors with small capacitance (3.6 μF for each one) are in parallel with the original capacitor (151 μF), as shown in Fig. 4(a) and Table IV. Then, these extra four capacitors are taken away one by one to simulate the degradation of capacitor (each one represents the drop of capacitance by 2.2%). In order to cover the fluctuations of the estimated results, the procedure shown in Fig. 3 is performed for 15 times with an individual recorded $i_{\rm L}$ and $v_{\rm o}$. Fig. 10 summarizes the estimated results. The simulated degradation levels of capacitor are indicated with the data clusters from C1 to C5. The operational cases are represented by different colors. The data with the same color represents the distribution of the estimated results at a given condition. Among them, the estimated L, $R_{\rm L}$, and $R_{\rm dson}$ are independent from the change of capacitance. While, for the capacitor related parameters, after taking away the paralleled capacitors one by one, although part of the data within the adjacent clusters are overlapped, collectively, the estimated cluster of capacitances decrease constantly. Meanwhile, the estimated $R_{\rm c}$ has a slightly increasing trend.

The self-heating can only increase the case temperature of capacitor $T_{\rm c}$ by 3 °C. Therefore, a heater is sticked on the surface of the capacitor to increase the $T_{\rm c}$ and to investigate the effect of the temperature on the proposed method. It can be seen from Fig. 11 that the capacitance is increased by only 2–3 μF when $T_{\rm c}$ is increased by 30 °C. While the perturbations of the estimated C and $R_{\rm c}$ are 9 μF and 0.4 Ω with increasing $T_{\rm c}$ by 30 °C, respectively. However, this perturbation is still within the perturbation of the results in Fig. 10. Thus, the proposed cluster-data based method is still effective when the $T_{\rm c}$ of capacitor is changed.

F. MOSFET Degradation Monitoring

Conventionally, the ON-state resistance of MOSFET $R_{\rm dson}$ is effective in indicating its health condition. As discussed before, the estimated $R_{\rm L}$ and $R_{\rm dson}$ fluctuate in a large range. Therefore,

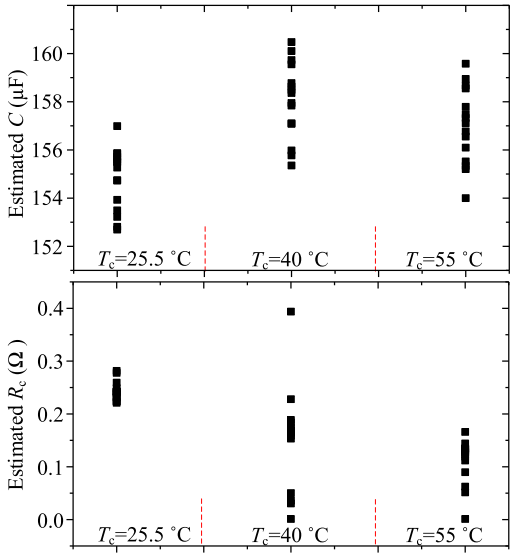

Fig. 11. Estimated C and R_c when case temperature T_c is changed (case 6).

it is challenging to monitor the degradation of MOSFET by using the estimated $R_{\rm dson}$ directly. However, according to Fig. 2 and (1), it can be seen that $R_{\rm L}$ and $R_{\rm dson}$ have almost same impact on $v_{\rm o}$ and $i_{\rm L}$, which means distinguishing them is virtually impossible. To overcome this challenge, a new equivalent period average resistance is proposed and defined as below to represent both $R_{\rm L}$ and $R_{\rm dson}$ in this article:

$$R_{\rm avg} = R_{\rm L} + DR_{\rm dson}. \tag{15}$$

D can be obtained from the digital twin controller. $R_{\rm dson}$ works only when the MOSFET is turned ON, while $R_{\rm L}$ works in the whole switching period. Therefore, $R_{\rm L}$ and $R_{\rm dson}$ can be represented by an equivalent average resistance $R_{\rm avg}$. To verify this, the estimated $R_{\rm L}$ and $R_{\rm dson}$ are illustrated in Fig. 12(a) and (b), respectively, which shows they fluctuate within a relative large range, but $R_{\rm avg}$ keeps stable within a relative small range, as shown in Fig. 12(c). In addition, it is worth to mentioning that inductor usually possesses very stable characteristics and its parameters are not changed during operation. Thus, $R_{\rm avg}$ enables the proposed method to monitor the degradation of MOSFET.

An accelerated power cycling platform was designed in [45], where $R_{\rm dson}$ is used as the indicator of aging process. In this article, $\Delta R_{\rm dson}$ reaches higher value before the MOSFETs actually fail (0.3–1 Ω). Usually, package related aging may only causes 5%–20% increase in $R_{\rm dson}$. Such higher increase shown in [45] is mainly due to the degradation of MOSFET chip as the significantly decrease of the gate-oxide capacitance, which results in the driving voltage drops lower than normal value. Then, the MOSFET operating in saturation region exhibits high output impedance [24]. Based on this, five MOSFETs with different $R_{\rm dson}$ are chosen in this article to simulate the degradation of MOSFET as listed in Table V (the $R_{\rm dson}$ of those MOSFETs are measured experimentally offline). The case temperature of the

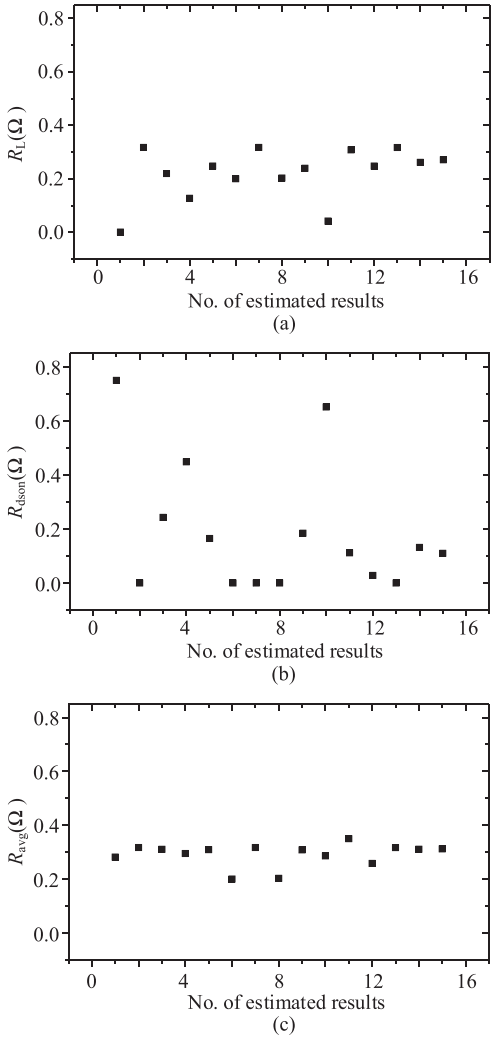

Fig. 12. Estimated parasitic resistances (the proposed calculation procedure is repeated for 15 times): (a) the parasitic resistance of inductor; (b) the ON-state resistance of MOSFET; (c) defined equivalent average resistance of $R_{\rm L}$ and $R_{\rm dson}$ by using equation (15).

MOSFETs in each operational condition is recorded as listed in Table VI, showing higher temperature with higher ON-state resistance, current, and duty cycle, such as those MOSFETs operating in case3. Then, the estimated results over different operational cases and MOSFETs are indicated with different colors and from M1 to M5, respectively, as shown in Fig. 13. The estimated L, C, and R_c are immune from the simulated degradation of MOSFET. While the estimated $R_{\rm avg}$ shows increasing trend from M1 to M5. Especially the relative large increment in case3 and case4 due to the higher temperature, which proves the ability of the proposed method in detecting the degradation progress of the MOSFET in a buck converter.

G. Simultaneous Degradation Test

In practice, the degradation of capacitor and MOSFET may happen simultaneously. Therefore, it is necessary to verify the

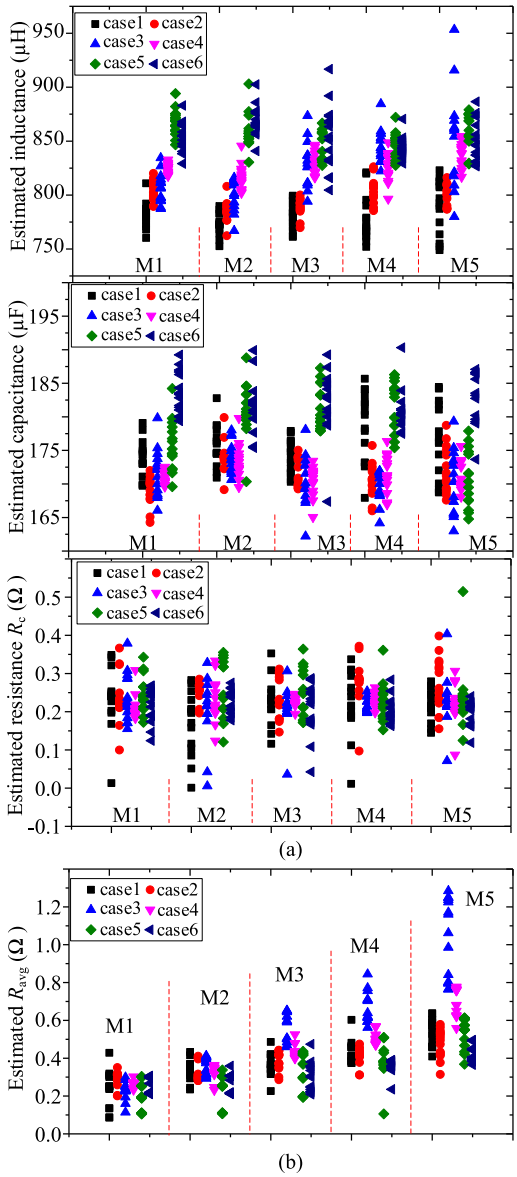

Fig. 13. Estimated results over different operational cases and simulated degradation levels of MOSFET (here the applied capacitor is 165 μF(C1). case 1-6 are described in Table III, the case temperature of MOSFETs are listed in Table VI, M1–M5 are described in Table V): (a) L, C, and R_c; (b) R_{avg}.

ability of the proposed method in monitoring the simultaneous degradation among these two key components. The estimated results are shown in Fig. 14, which proves the degradation trend of capacitor and MOSFET can be identified simultaneously by the proposed method.

H. Data Analysis

Due to the variations from the measurement errors, the temperature factors, and the workloads, the component parameters are obtained as a data cluster. To provide an evaluation standard, the boxplot technique is applied to derive the statistical measures of the data cluster so as to quantify the degradation levels.

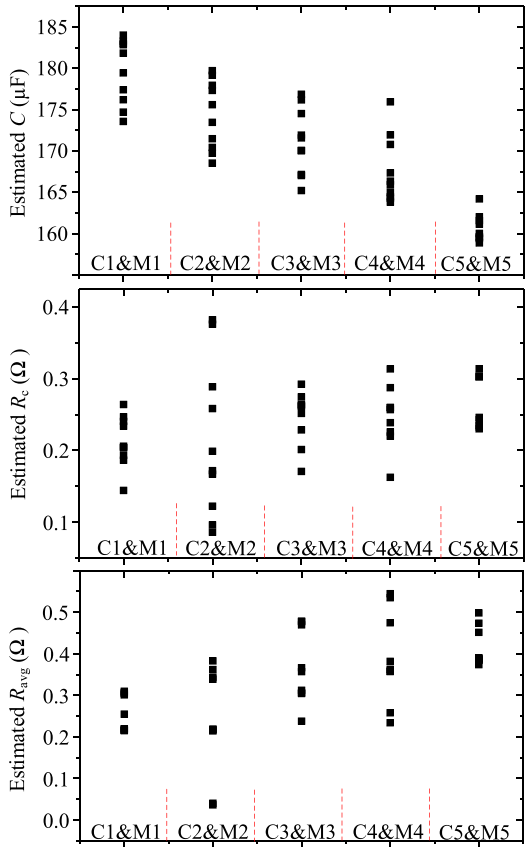

Fig. 14. Estimated C, R_c and R_{avg} when capacitor and MOSFET are degraded simultaneously (case6) (M1–M5 are described in Table. V, C1–C5 are described in Table IV).

Boxplot technique is an effective method for the representation of data structure by calculating the statistics including median and quantiles, based on which the degradation trend can be clearly determined. With the data clusters in Fig. 10(d), (e), and 13(b), the respective boxplots of these clusters are calculated and shown in Figs. 15 and 16. As can be seen, there is a clear degradation trend according to the medians of the data cluster, and the details are given in Table VII. Those outliers are those data is out of 95% confidence interval and the existing of those outliers is reasonable due to the experimental noise. The more narrower box means the data are more concentrated. Specifically, the estimated medians of C and R_c are decreased by 9.7% and increased by 21%, respectively, when the capacitor is degraded by 8.8%. Meanwhile, the median of R_{avg} is increased from 0.243 Ω to 0.561 Ω when the R_{dson} is manually increased from 0.11 Ω to 0.75 Ω. Although the estimated parameters are not quite close to the real ones, the relative degradation change of each parameter can be identified, which demonstrates that the proposed method is effective in monitoring the degradation level of the key components in buck converters.

The buck converter is considered as the simplest topology to prove the proposed concept of this article. Nevertheless, it represents the features of many other buck-type converters and voltage-source inverters. Therefore, the applicability of the same

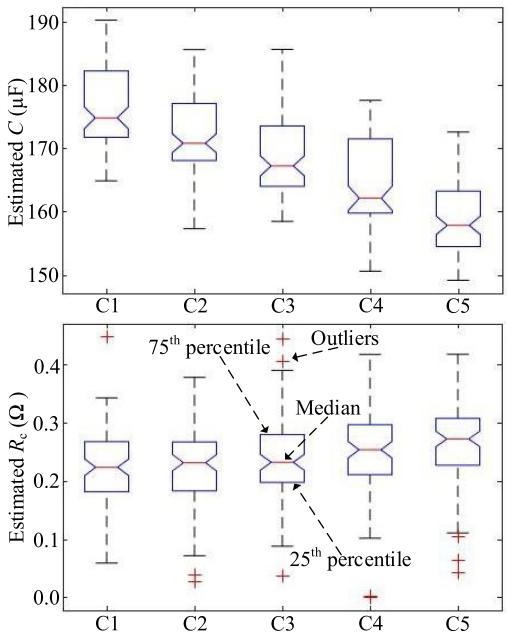

Fig. 15. Probability density distribution of the estimated C and R_c of all obtained data from case 1 to case 7 (C1–C5 are described in Table IV).

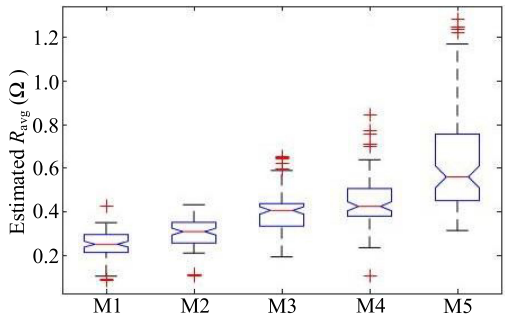

Fig. 16. Probability density distribution of the estimated R_{avg} of all obtained data from case 1 to case 7 (M1–M5 are described in Table V).

TABLE VII
OBTAINED MEDIAN VALUE OF THE IDENTIFIED PARAMETERS AFTER DATA PROCESS

Median (Cap)	C1	C2	C3	C4	C5
C (μF)	174.9	170.9	167.3	162.2	158
R_c (mΩ)	224	232	233	254	273
Median (MOS)	M1	M2	M3	M4	M5
R_{avg} (mΩ)	252	310	407	426	561

concept for single-phase inverters and three-phase inverters can also be expected in the future. Even though, various challenges still need to be further solved.

V. CONCLUSION

In this article, a digital twin concept-based condition monitoring method is proposed and verified through a buck converter case study. The experimental tests are performed to verify its feasibility and the results show that the digital twin of the buck converter can achieve similar output waveforms (inductor current i_{L} and output voltage v_{o}) with the physical buck converter. Then, practical considerations are discussed (impact of sampling rate, different operation conditions, temperature and the uncertainty caused by errors). To avoid calibrating the relationship between the health indicator and their impact factors, a cluster-data based method is used in this article. Finally, the capability of monitoring the degradation of key components (capacitor and MOSFET) in converter is verified experimentally. When the capacitance is decreased by 2.2% for each step, the identified cluster of capacitances are able to indicate the degradation process. For MOSFET, the identified R_{dson} cannot be used directly to indicate the degradation of MOSFET. To overcome this, a new equivalent resistance between R_{L} and R_{dson} are defined in this article as R_{avg}. Similarly, by calculating a cluster of this new defined resistance, the increase of R_{dson} can be identified. Finally, the probability density distribution-based data process method is used to achieve the characteristic value of each cluster-data which can be used as the final degradation level indicator. For implementation, three signals need to be measured from the physical buck converter by using regular sensors: inductor current, output voltage and input voltage. In addition, dynamic waveforms are prerequisite for this method, which can be achieved from the load change events, input voltage change transient, start-up and shut-down transient.

In conclusion, the feasibility and effectiveness of the proposed method in monitoring the degradation level of capacitor and MOSFET are proved experimentally and practical issues are also considered. Compare to conventional methods, the proposed method provides a feasible and practical solution for condition monitoring of power converter with superiorities in noninvasive, calibration-free, and without additional hardware circuits.

REFERENCES

[1] S. Dusmez and B. Akin, "An accelerated thermal aging platform to monitor fault precursor on-state resistance," in *Proc. IEEE Int. Electric Mach. Drives Conf.*, May 2015, pp. 1352–1358.
[2] M. A. Vogelsberger, T. Wiesinger, and H. Ertl, "Life-cycle monitoring and voltage-managing unit for dc-link electrolytic capacitors in PWM converters," *IEEE Trans. Power Electron.*, vol. 26, no. 2, pp. 493–503, Feb. 2011.
[3] H. Oh, B. Han, P. McCluskey, C. Han, and B. D. Youn, "Physics-of-failure, condition monitoring, and prognostics of insulated gate bipolar transistor modules: A review," *IEEE Trans. Power Electron.*, vol. 30, no. 5, pp. 2413–2426, May 2015.
[4] S. Yang, D. Xiang, A. Bryant, P. Mawby, L. Ran, and P. Tavner, "Condition monitoring for device reliability in power electronic converters: A review," *IEEE Trans. Power Electron.*, vol. 25, no. 11, pp. 2734–2752, Nov. 2010.
[5] H. Soliman, H. Wang, and F. Blaabjerg, "A review of the condition monitoring of capacitors in power electronic converters," *IEEE Trans. Ind. Appl.*, vol. 52, no. 6, pp. 4976–4989, Nov. 2016.
[6] U. Choi, S. JÃrgensen, and F. Blaabjerg, "Advanced accelerated power cycling test for reliability investigation of power device modules," *IEEE Trans. Power Electron.*, vol. 31, no. 12, pp. 8371–8386, Dec. 2016.
[7] S. Beczkowski, P. Ghimre, A. R. de Vega, S. Munk-Nielsen, B. Rannestad, and P. Thogersen, "Online VCE measurement method for wear-out monitoring of high power IGBT modules," in *Proc. 15th Eur. Conf. Power Electron. Appl.*, Sep. 2013, pp. 1–7.
[8] B. Ji *et al.*, "In situ diagnostics and prognostics of solder fatigue in igbt modules for electric vehicle drives," *IEEE Trans. Power Electron.*, vol. 30, no. 3, pp. 1535–1543, Mar. 2015.

[9] D. Astigarraga *et al.*, "Analysis of the results of accelerated aging tests in insulated gate bipolar transistors," *IEEE Trans. Power Electron.*, vol. 31, no. 11, pp. 7953–7962, Nov. 2016.
[10] X. Ye, C. Chen, Y. Wang, G. Zhai, and G. J. Vachtsevanos, "Online condition monitoring of power mosfet gate oxide degradation based on miller platform voltage," *IEEE Trans. Power Electron.*, vol. 32, no. 6, pp. 4776–4784, Jun. 2017.
[11] J. Liu, G. Zhang, Q. Chen, L. Qi, Y. Geng, and J. Wang, "In situcondition monitoring of IGBTS based on the miller plateau duration," *IEEE Trans. Power Electron.*, vol. 34, no. 1, pp. 769–782, Jan. 2019.
[12] C. H. van der Broeck, A. Gospodinov, and R. W. De Doncker, "IGBT junction temperature estimation via gate voltage plateau sensing," *IEEE Trans. Ind. Appl.*, vol. 54, no. 5, pp. 4752–4763, Sep. 2018.
[13] R. Mandeya, C. Chen, V. Pickert, and R. T. Naayagi, "Prethreshold voltage as a low-component count temperature sensitive electrical parameter without self-heating," *IEEE Trans. Power Electron.*, vol. 33, no. 4, pp. 2787–2791, Apr. 2018.
[14] N. Baker, S. Munk-Nielsen, F. Iannuzzo, and M. Liserre, "IGBT junction temperature measurement via peak gate current," *IEEE Trans. Power Electron.*, vol. 31, no. 5, pp. 3784–3793, May 2016.
[15] H. Luo, Y. Chen, P. Sun, W. Li, and X. He, "Junction temperature extraction approach with turn-off delay time for high-voltage high-power igbt modules," *IEEE Trans. Power Electron.*, vol. 31, no. 7, pp. 5122–5132, Jul. 2016.
[16] H. Niu and R. D. Lorenz, "Sensing power mosfet junction temperature using gate drive turn-on current transient properties," *IEEE Trans. Ind. Appl.*, vol. 52, no. 2, pp. 1677–1687, Mar. 2016.
[17] Z. Wang, B. Tian, W. Qiao, and L. Qu, "Real-time aging monitoring for igbt modules using case temperature," *IEEE Trans. Ind. Electron.*, vol. 63, no. 2, pp. 1168–1178, Feb. 2016.
[18] D. Xiang, L. Ran, P. Tavner, A. Bryant, S. Yang, and P. Mawby, "Monitoring solder fatigue in a power module using case-above-ambient temperature rise," *IEEE Trans. Ind. Appl.*, vol. 47, no. 6, pp. 2578–2591, Nov. 2011.
[19] W. Lai, M. Chen, L. Ran, O. Alatise, S. Xu, and P. Mawby, "Low δt_j stress cycle effect in igbt power module die-attach lifetime modeling," *IEEE Trans. Power Electron.*, vol. 31, no. 9, pp. 6575–6585, Sep. 2016.
[20] Y. Wu and X. Du, "A ven condition monitoring method of dc-link capacitors for power converters," *IEEE Trans. Ind. Electron.*, vol. 66, no. 2, pp. 1296–1306, Feb. 2019.
[21] N. Agarwal, M. W. Ahmad, and S. Anand, "Quasi-online technique for health monitoring of capacitor in single-phase solar inverter," *IEEE Trans. Power Electron.*, vol. 33, no. 6, pp. 5283–5291, Jun. 2018.
[22] A. Wechsler, B. C. Mecrow, D. J. Atkinson, J. W. Bennett, and M. Benarous, "Condition monitoring of dc-link capacitors in aerospace drives," *IEEE Trans. Ind. Appl.*, vol. 48, no. 6, pp. 1866–1874, Nov. 2012.
[23] Y. Jo, T. H. Nguyen, and D. Lee, "Condition monitoring of submodule capacitors in modular multilevel converters," in *Proc. IEEE Energy Convers. Congr. Expo.*, Sep. 2014, pp. 2121–2126.
[24] S. Dusmez, M. Bhardwaj, L. Sun, and B. Akin, "In situ condition monitoring of high-voltage discrete power mosfet in boost converter through software frequency response analysis," *IEEE Trans. Ind. Electron.*, vol. 63, no. 12, pp. 7693–7702, Dec. 2016.
[25] D. Xiang, L. Ran, P. Tavner, S. Yang, A. Bryant, and P. Mawby, "Condition monitoring power module solder fatigue using inverter harmonic identification," *IEEE Trans. Power Electron.*, vol. 27, no. 1, pp. 235–247, Jan. 2012.
[26] A. Soualhi *et al.*, "Heath monitoring of capacitors and supercapacitors using the neo-fuzzy neural approach," *IEEE Trans. Ind. Informat.*, vol. 14, no. 1, pp. 24–34, Jan. 2018.
[27] H. Soliman, H. Wang, B. Gadalla, and F. Blaabjerg, "Condition monitoring for dc-link capacitors based on artificial neural network algorithm," in *Proc. IEEE 5th Int. Conf. Power Eng., Energy Elect. Drives*, May 2015, pp. 587–591.
[28] M. Algreer, M. Armstrong, and D. Giaouris, "Active online system identification of switch mode dc-dc power converter based on efficient recursive DCD-IIR adaptive filter," *IEEE Trans. Power Electron.*, vol. 27, no. 11, pp. 4425–4435, Nov. 2012.
[29] M. Ahmeid, M. Armstrong, S. Gadoue, M. Al-Greer, and P. Missailidis, "Real-time parameter estimation of dc-dc converters using a self-tuned kalman filter," *IEEE Trans. Power Electron.*, vol. 32, no. 7, pp. 5666–5674, Jul. 2017.
[30] B. X. Li and K. S. Low, "Low sampling rate online parameters monitoring of dc-dc converters for predictive-maintenance using biogeography-based optimization," *IEEE Trans. Power Electron.*, vol. 31, no. 4, pp. 2870–2879, Apr. 2016.
[31] J. Poon, P. Jain, C. Spanos, S. K. Panda, and S. R. Sanders, "Fault prognosis for power electronics systems using adaptive parameter identification," *IEEE Trans. Ind. Appl.*, vol. 53, no. 3, pp. 2862–2870, May 2017.
[32] A. Alghassi, S. Perinpanayagam, M. Samie, and T. Sreenuch,"Computationally efficient, real-time, and embeddable prognostic techniques for power electron.," *IEEE Trans. Power Electron.*, vol. 30, no. 5, pp. 2623–2634, May 2015.
[33] S. H. Ali, M. Heydarzadeh, S. Dusmez, X. Li, A. S. Kamath, and B. Akin, "Lifetime estimation of discrete IGBT devices based on Gaussian process," *IEEE Trans. Ind. Appl.*, vol. 54, no. 1, pp. 395–403, Jan. 2018.
[34] A. Parrott and L. Warshaw (2017, Aug.) Industry 4.0 and the digital twin. [Online]. Available: https://www2.deloitte.com/content/dam/Deloitte/cn/Documents/cip/deloitte-cn-cip-industry-4-0-digital-twin-technology-en-171215.pdf
[35] O. white paper (2017) Digital twin for iot applications. [Online]. Available: http://www.oracle.com/us/solutions/internetofthings/digital-twins-for-iot-apps-wp-3491953.pdf
[36] M. Milton, C. A. De La O, H. L. Ginn, and A. Benigni, "Controller-embeddable probabilistic real-time digital twins for power electronic converter diagnostics," *IEEE Trans. Power Electron.*, vol. 35, no. 9, pp. 9850–9864, Sep. 2020.
[37] P. Jain, J. Poon, J. P. Singh, C. Spanos, S. R. Sanders, and S. K. Panda, "A digital twin approach for fault diagnosis in distributed photovoltaic systems," *IEEE Trans. Power Electron.*, vol. 35, no. 1, pp. 940–956, Jan. 2020.
[38] Y. Peng and H. Wang, "Application of digital twin concept in condition monitoring for dc-dc converters," in *Proc. IEEE Energy Convers. Congr. Expo.*, Oct. 2019, pp. 2199–2204.
[39] J. Hult, "A fourth order Runge Kutta in the interaction picture method for simulating supercontinuum generation in optical fibers," *J. Lightw. Technol.*, vol. 25, no. 12, pp. 3770–3775, Dec. 2007.
[40] J. W. Kimball and P. T. Krein, "A current-sensorless digital controller for active power factor correction control based on Kalman filters," in *Proc. 23rd Annu. IEEE Appl. Power Electron. Conf. Expo.*, 2008, pp. 1328–1333.
[41] P. Dash and R. Mallick, "Accurate tracking of harmonic signals in VSC-HVDC systems using PSO based unscented transformation," *Int. J. Elect. Power Energy Syst.*, vol. 33, no. 7, pp. 1315–1325, 2011.
[42] S. Bolognani, L. Tubiana, and M. Zigliotto, "Extended Kalman filter tuning in sensorless PMSM drives," *IEEE Trans. Ind. Appl.*, vol. 39, no. 6, pp. 1741–1747, Nov./Dec. 2003.
[43] Z. Zhan, J. Zhang, Y. Li, and H. S. Chung, "Adaptive particle swarm optimization," *IEEE Trans. Syst., Man, Cybern., Part B*, vol. 39, no. 6, pp. 1362–1381, Dec. 2009.
[44] W. Wang, A. C. Liu, H. S. Chung, R. W. Lau, J. Zhang, and A. W. Lo, "Fault diagnosis of photovoltaic panels using dynamic current-voltage characteristics," *IEEE Trans. Power Electron.*, vol. 31, no. 2, pp. 1588–1599, Feb. 2016.
[45] S. Dusmez, H. Duran, and B. Akin, "Remaining useful lifetime estimation for thermally stressed power mosfets based on on-state resistance variation," *IEEE Trans. Ind. Appl.*, vol. 52, no. 3, pp. 2554–2563, May 2016.

Yingzhou Peng (Student Member, IEEE) received the B.S. degree in electrical engineering from the Harbin Engineering University, Harbin, China, in 2014, and the M.S. degree in power electronics from Chongqing University, Chongqing, China, in 2017. He is currently working toward the Ph.D. degree with Aalborg University, Aalborg, Denmark.

He was a Visiting Researcher with the Electrical Power and Energy Conversion Lab, Cambridge University, Cambridge, U.K, in 2020. His research interests include the failure mechanisms analysis of power electronic components, the improvement of the robustness and reliability of power converters by means of condition monitoring.

Shuai Zhao (Member, IEEE) received the B.S. degree in telcommunication engineering, the M.S. degree in telcommunication and information system, and the Ph.D. degree in information and telcommunication engineering from Northwestern Polytechnical University, Xi'an, China, in 2011, 2014, and 2018, respectively.

He is currently a Postdoctoral Researcher with the Center of Reliable Power Electronics (CORPE), Department of Energy Technology, Aalborg University, Denmark. From 2014 to 2016, he was a Visiting Ph.D. Student with the Department of Mechanical and Industrial Engineering, University of Toronto, Toronto, ON, Canada, with the scholarship from China Scholarship Council (CSC). In August 2018, he was a Visiting Scholar with the Power Electronics and Drives Laboratory, Department of Electrical and Computer Science, University of Texas at Dallas, Richardson, TX, USA. His research interests include condition monitoring, data analytics, machine learning, anomaly detection, diagnostics and prognostics of power electronic systems.

Huai Wang (Senior Member, IEEE) received the B.E. degree in electrical engineering from the Huazhong University of Science and Technology, Wuhan, China, in 2007, and the Ph.D. degree in power electronics, from the City University of Hong Kong, Hong Kong, in 2012.

He is currently a Professor with the Center of Reliable Power Electronics (CORPE), Department of Energy Technology, Aalborg University, Denmark. He was a Visiting Scientist with the ETH Zurich, Switzerland, from August to September 2014, and with the Massachusetts Institute of Technology (MIT), USA, from September to November 2013. He was with the ABB Corporate Research Center, Switzerland, in 2009. His research addresses the fundamental challenges in modeling and validation of power electronic component failure mechanisms, and application issues in system-level predictability, condition monitoring, circuit architecture, and robustness design.

Dr. Wang was a recipient of the Richard M. Bass Outstanding Young Power Electronics Engineer Award from the IEEE Power Electronics Society in 2016, and the Green Talents Award from the German Federal Ministry of Education and Research in 2014. He is currently the Chair of IEEE PELS/IAS/IES Chapter in Denmark. He serves as an Associate Editor for the *IET Electronics Letters*, IEEE JOURNAL OF EMERGING AND SELECTED TOPICS IN POWER ELECTRONICS, and IEEE TRANSACTIONS ON POWER ELECTRONICS.